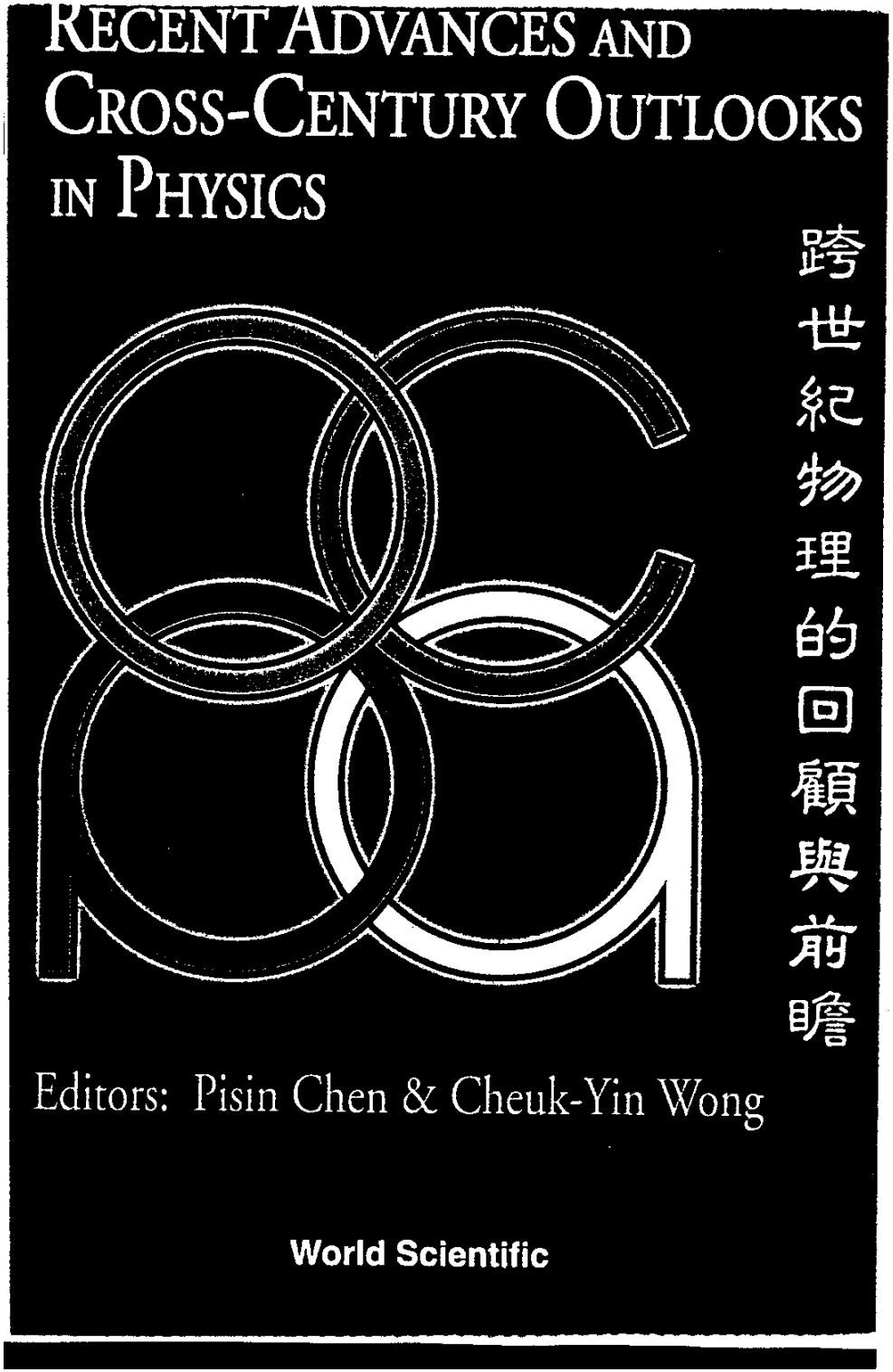

RECENT ADVANCES AND CROSS-CENTURY OUTLOOKS IN PHYSICS

Interplay between Theory and Experiment

跨世紀物理的回顧與前瞻

理論與實驗的互動

Proceedings of the Conference held on March 18–20, 1999 in Atlanta, Georgia

Sponsored by
Overseas Chinese Physics Association
National Science Council
National Center for Theoretical Sciences

Editors

Pisin Chen
Stanford Linear Accelerator Center
Stanford University
Stanford, California 94309

Cheuk-Yin Wong
Physics Division
Oak Ridge National Laboratory
Oak Ridge, Tennessee 37831

World Scientific
Singapore • New Jersey • London • Hong Kong

RECENT ADVANCES IN GYROTRON TRAVELING WAVE AMPLIFIER

K.R. CHU, T.H. CHANG, H.Y. CHEN, C.L. HUNG, and L.R. BARNETT
Department of Physics, National Tsing Hua University, Hsinchu, Taiwan
E-mail: krchu@phys.nthu.edu.tw

S.H. CHEN
National Center for High-Performance Computing, Hsinchu, Taiwan

T.T. YANG
Synchrotron Radiation Research Center, Hsinchu, Taiwan

Stability issues comprise the key factors limiting the performance of the gyrotron traveling wave amplifier (gyro-TWT), a promising source of high power millimeter waves based on the relativistic electron cyclotron maser instability. We present a brief review of recent progress made on the stability studies of the gyro-TWT. Physical origins of spurious oscillations in the gyro-TWT are analyzed and characterized. Fundamental understanding of these processes leads to a device concept which provides zero-drive stability at ultra high gain. The scheme was verified in a proof-of-principle experiment, the results of which significantly advanced the state-of-the-art of millimeter wave amplifiers in gain, power, bandwidth, and efficiency.

I. Introduction

The millimeter wave region of the electromagnetic spectrum is a relatively unexploited band between the microwave and optical frequencies. A myriad of applications [1] of millimeter waves, such as high resolution radars, long range and high directivity communications, atmospheric mapping, space object detection and identification, and advanced particle accelerators are being conceived which require powerful sources well beyond currently available technology. The electron cyclotron maser mechanism discovered in the 1950's [2-4] has since evolved from a basic relativistic physics effect into a new class of millimeter wave devices referred to as the gyrotron. Consider an electron beam in which electrons move in helical orbits in an external magnetic field. Because of the relativistic mass dependence of the cyclotron frequency, the electrons in the RF field will bunch in their gyrotional phase space and thereby amplify the RF field which causes the bunching to occur. The gyrotron traveling wave amplifier (gyro-TWT) is an amplifier version of the gyrotron which features a fast-wave structure for high-power and broad-band interaction [5]. Table 1 summarizes the achieved gyro-TWT performances [6-12] over a twenty-year period of research and development. The current paper, mostly based on Refs. 11 and

Table 1. Achieved performance of gyro-TWT's based on a weakly relativistic electron beam

year	institution (references)	cyclotron harmonic	voltage (kV)	center frequency (GHz)	3dB bandwidth (%)	peak power (kW)	saturated gain (dB)	efficiency (%)
1979	NRL (6)	1	70	35	1.5	16.6	20	7.8
1981	Varian (7)	1	60	5	6	120	18	26
1982	Varian (8)	1	50	95	2	28	33	8
1993	NRL (9)	1	33	35	20	8	25	16
1994	UC Davis (10)	2	80	16	2.1	207	16	13
1998	NTHU (11, 12)	1	100	35	8.6	93	70	26.5

12, reviews the key physics issues of the gyro-TWT as well as the experimental demonstration of the gyro-TWT as a millimeter wave amplifier of unprecedented capabilities in power, gain, bandwidth, and efficiency.

In contrast to conventional linear beam microwave devices such as the traveling wave tube (TWT), the electron beam employed in the gyrotron possesses a transverse motion at the electron cyclotron frequency. It is this property that allows the beam to selectively interact with a high order waveguide mode at a high cyclotron harmonic by properly matching the resonance conditions. However, the additional degree of freedom provided by the multitude of cyclotron harmonics can also generate numerous spurious oscillations. Interactions with backward waves are sources of absolute instabilities [13-18], whereas the forward wave interactions are normally, but not always, convective instabilities [18]. The gyro-TWT is a complicated case because it exploits a convective instability near the cutoff frequency which turns into an absolute instability at sufficiently high beam current when the unstable spectrum extends into the backward wave region. These various absolute instabilities can easily be the dominant sources of oscillations in the gyro-TWT.

Feedback due to reflections at structural nonunifomities presents a different source of oscillation in the high gain regime (referred to as the reflective oscillation). Reflective oscillations are common in traveling wave structures. The feedback loop can be effectively eliminated by a sever as has been a standard practice in TWTs. However, the absolute instability, a much more serious problem to the gyro-TWT than to the conventional TWT, is basically different from the reflective oscillation in that the backward wave associated with the absolute instability is internally generated by the ac electron beam current. Hence, the two stages, though separated by the sever, are coupled by the beam. With the beam providing an internal path, the sever does

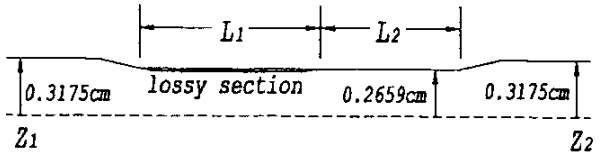

Fig. 1. Schematic of a Ka-band, TE_{11} mode, fundamental harmonic gyro-TWT. Section L_1 and L_2 form the interaction region. The ends are tapered for broadband coupling.

not really quite separate the interaction structure into two isolated sections to produce a substantial stabilizing effect. Recently, an interaction structure with distributed wall losses was shown to be effective in suppressing both types of oscillations [19]. The losses are distributed over much of the linear interaction region (Fig. 1). Like the sever, the lossy section cuts off the path of the reflective feedback loop . In contrast to the sever, however, it is an integral part of the linear amplification stage. To the predominantly backward power flow of the absolute instability, the lossy section also functions as an effective energy sink.

II. A Scheme for Ultra High Gain

The distributed-loss structure can also yield ultra high stable gain [11, 12]. The scheme is based on the different responses to wall losses between the cold tube and hot tube modes. The cold tube mode has all of its energy in the electromagnetic fields. In a hot tube, however, energy of the beam generated mode resides not only in the electromagnetic fields but also in the kinetic energy of the oscillatory motion of the electrons, the latter being an integral part of the hot tube mode. The lossy wall absorbs the electromagnetic energy, but not the oscillatory energy of the electrons. Thus, wall losses of the amplifier circuit attenuate the reflected wave (basically a cold tube mode) significantly more than they reduce the gain of the amplifying wave (a hot tube mode). It can be shown analytically [20] that the reduction in hot tube gain due to wall losses is only one third of the cold tube attenuation over the same distance.

Such unequal effects can be exploited to simultaneously achieve both high gain and reflective stability. In Fig. 1, the lossy and conducting-wall sections comprise the linear and nonlinear stages of the amplification, respectively. The linear section is made sufficiently long to provide the desired gain, while the nonlinear section length

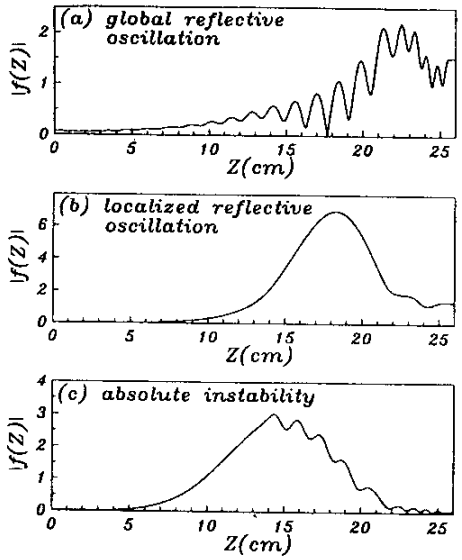

Fig. 2. Calculated profiles of the RF field amplitude $|f(z)|$ in the structure of Fig. 1 for A. the global reflective oscillation, B. the localized reflective oscillation, and C. the absolute instability.

is constrained to a minimum to enhance the threshold of absolute instabilities.

III. Classification and Characterization of Oscillations

We first discuss three types of oscillations studied in Refs. 11 and 12 by employing the trajectory tracing technique [21-24] to follow the beam and wave dynamics throughout the lossy section. Imposition of physical boundary conditions at both ends allows the evaluation of a self-consistent rf field profile, f(z), to account for wave reflections at all interfaces and nonuniformities. Such details in the modeling allow oscillations of various origins to be studied on the basis of the overall rather than sectionalized interaction structure.

Reflective oscillations of a global nature start when the total gain exceeds the reflection at the input/output ends plus the attenuation in the lossy section (all in dB). Figure 2a shows the field profile of a typical global reflective oscillation.

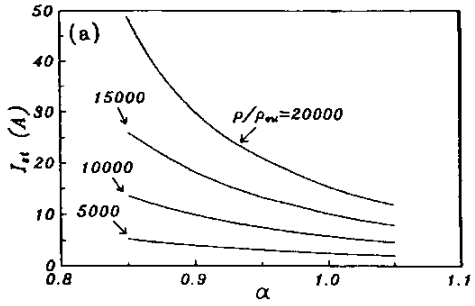

Fig. 3. Calculated start-oscillation current of the second harmonic absolute instability (TE_{21} mode, f_{osc} ≅56 GHz) versus the electron pitch angle α for different values of wall resistivity ρ (normalized to that of copper). V_b =100 kV, L_1=10 cm, L_2=9.7 cm, B_o=12.5 kG, and r_c=0.09 cm, where r_c is the radial position of the electron guiding centers. A cold beam is assumed.

Calculations indicate that the oscillation can be stabilized by lowering the operating current (I_b) and magnetic field (B_o), or by increasing the wall resistivity. Beam current is usually fixed by the power requirement and the magnetic field must be fine tuned for maximum efficiency; hence, wall resistivity provides the most effective means for stabilization. Wall resistivity reduces the gain, but this can be easily compensated by a lengthened lossy section.

The conducting-wall section (of length L_2 in Fig. 1) by itself is subject to localized oscillations due to reflections at the lossy-wall junction on the left and the output structure on the right. Figure 2b illustrates the field profile of such an oscillation in the lowest order (TE_{111}) axial mode. Since the oscillation is localized to the conducting-wall section, the oscillation power is found to be nearly independent of the length (L_1) and wall resistivity (ρ) of the lossy section. These two features are in contrast to the high sensitivity of the global reflective oscillation to L_1 and ρ.

The gyro-TWT shown in Fig. 1 is most susceptible to the TE_{21} mode absolute instability at the second cyclotron harmonic (14). Figure 2c illustrates the field profile of such an oscillation. Figure 3 displays the start-oscillation current (I_{st}) versus the electron pitch angle $\alpha(= v_\perp / v_z)$ for different values of ρ. I_{st} decreases with increasing α as expected. Again, the wall resistivity is shown to be highly effective in stabilizing the absolute instability. Increasing the wall resistivity will allow stable operation at higher I_b and α values, hence achieve higher power and efficiency.

Of the three types of oscillations, only the localized reflective oscillation cannot

Fig. 4. Photo of the Ka-band gyro-TWT detached from the superconducting magnet.

be effectively suppressed by distributed wall losses. It has indeed been observed in the experiment described below, but at a magnetic field value above the optimum range for the amplifier operation.

IV. Experiments

An experimental gyro-TWT [11, 12] (photo shown in Fig. 4) was assembled to verify the ultra high gain scheme just described. A mechanically tunable magnetron injection electron gun [25] was attached to the interaction structure of Fig. 1. Lengths of the graphite-coated lossy section (L_1=20 cm with~100 dB loss) and the conducting-wall section (L_2=4 cm) were chosen to achieve high gain as well as stability. Input/output waves were coupled at z_1 and z_2 through the side walls with newly designed oscillation-free couplers which also function as converters between circularly and linearly polarized waves. The magnetic field was provided by a superconducting magnet system. Output power at low duty was measured with a calibrated crystal detector (with estimated accuracy of ±5%) and verified with a calorimeter (agreement was within ~5%). At the operating beam current of 3.5 A, the gyro-TWT was found to be zero-drive stable from all three types of instabilities in the optimum range of the operating magnetic field (12.65kG<B_o<12.75kG). As the magnetic field was increased, a localized reflective oscillation was observed and identified to be the TE_{111} mode of the conducting-wall section.

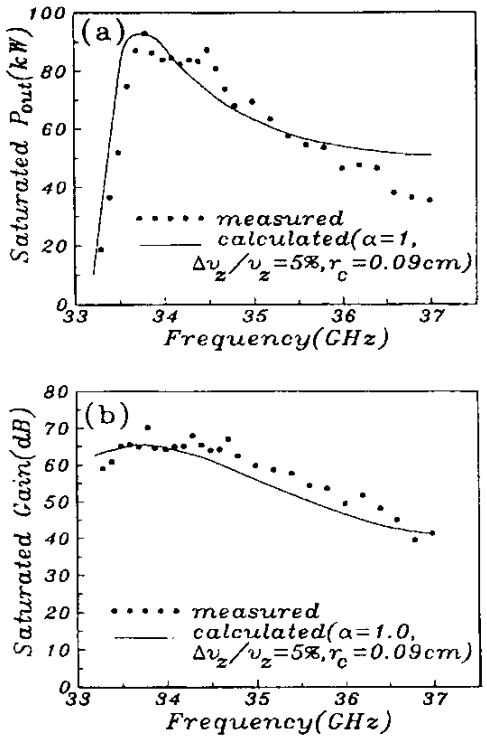

Fig. 5. Saturated output power (A) and gain (B) versus the frequency. Measured and calculated data are shown by dots and lines, respectively. V_b =100 kV, I_b=3.5 A, and B_o=12.7 kG.

Figure 5 plots the saturated output power and gain (dots) as functions of the frequency. The peak power of 93 kW corresponds to a saturated gain of 70 dB and efficiency of 26.5%. The ultra high gain, 30 dB beyond that previously achieved (Table 1), permits the use of solid state sources as drives. The full-width half-maximum bandwidth is 3 GHz, approximately 8.6% of the center frequency. Measured data are closely matched by theoretical predictions (solid line) using the simulated beam parameters (23) α=1, $\Delta v_z / v_z$ = 5% and r_c=0.09 cm, where $\Delta v_z / v_z$ is the electron velocity spread and r_c is the radial position of the electron guiding centers. The theory also predicts that the saturated power is almost independent of the length of the lossy section while the gain is linearly proportional to it. The peak Ohmic power dissipated on the waveguide is calculated to be

Table 2. Comparison of the experimental gyro-TWT with the state-of-the-art TWT (Varian/CPI model VTA 5701)

type	band	voltage (kV)	current (Amp)	magnet	peak power (kW)	efficiency (%)	gain (dB)	bandwidth (%)
gyro-TWT	Ka	100	3.5	cryogenic	93	26.5	70	8.6
TWT	Ka	45	7	solenoid	50	16	40	6

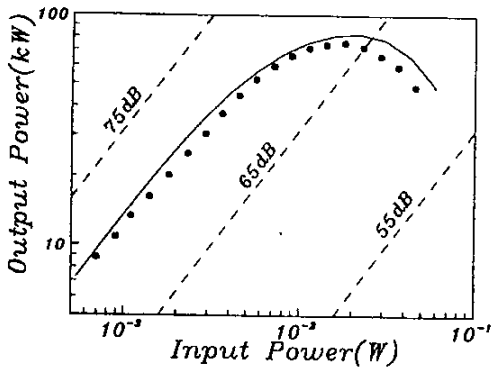

Fig. 6. Measured (dots) and calculated (lines) output power versus the drive power. V_b =100 kV, I_b=3.5 A, B_o=12.7 kG, and f=34.2 GHz.

approximately 10 kW. With profiled wall losses, it can be evenly distributed over the lossy surface area with a peak dissipation rate of ~300 W/cm^2. The average-power handling capability will be limited by the availability of proper heat-resistant lossy materials and advanced cooling techniques. However, supplementary attenuation by broadband side-wall coupling to an external load could conceivably be implemented to remove this limitation.

Figure 6 shows the measured output power versus the input power (dots). Linear and saturated behaviors are consistent with the calculated data (solid line). Again, α=1, $\Delta v_z / v_z = 5\%$, and r_c=0.09 cm were assumed in the calculations. In all the measurements for Figs.5 and 6, we have not detected any spurious oscillation. Table 2 compares the key parameters of the current gyro-TWT with those of the state-of-the-art TWT.

V. Summary

These studies indicate that a basic understanding of the intricate interplay between the absolute/convective instabilities, circuit losses, and reflective feedback is of fundamental importance to the scientific demonstration of the potential capability of the gyro-TWT. Significantly higher power can be obtained by employing the harmonic cyclotron maser interaction [10, 26] and these new physical insights, thereby ushering in a new generation of coherent millimeter wave amplifiers.

Acknowledgements

This work was supported by the National Science Council. The authors are grateful for many stimulating discussions with Prof. Neville C. Luhmann, Jr.

References

1. A.V. Gaponov-Grekhov, V.L. Granatstein, Eds. *Application of High Power Microwaves* (Artech House, Boston, MA, 1994).
2. R.Q. Twiss, *Australian J. Phys.* **11**, 564 (1958).
3. J. Schneider, *Phys. Rev. Lett.* **2**, 504 (1959).
4. A.V. Gaponov, *Izv, VUZ, Radiofizika* **2**, 450 (1959), ibid., p.836.
5. V.L. Granatstein, P. Sprangle, A.T. Drobot, K.R. Chu, and L. Seftor, U.S. patent no. 4224576 (1980).
6. L.R. Barnett et al., in *Technical Digest of the International Electron Devices Meeting* (IEEE, New York, 1979), pp.164-167.
7. R.S. Symons, H.R. Jory, S.J. Hegji, and P.E. Ferguson, *IEEE Trans. Microwave Theory Tech.* **29**, 181 (1981).
8. V.L. Granatstein, B. Levush, B.G. Danly, and R.K. Parker, *IEEE Trans. Plasma Sci.* **25**, 1322 (1997).
9. G.S. Park et al., *Phys. Rev. Lett.* 77, 2399 (1995).
10. Q.S. Wang, D.B. McDermott, and N.C. Luhmann, Jr., *Phys. Rev. Lett.* **75**, 4322 (1995).
11. K.R. Chu, H.Y. Chen, C.L. Hung, T.H. Chang, L.R. Barnett, S.H. Chen, and T.T. Yang, Phys. Rev. Lett. 81, 4760 (1998).
12. K.R. Chu, H.Y. Chen, C.L. Hung, T.H. Chang, L.R. Barnett, S.H. Chen, T.T. Yang, and D. Dialetis, IEEE Trans. Plasma Sci. (April, 1999).

13. Y.Y. Lau, K.R. Chu, L.R. Barnett, and V.L. Granatstein., *Int. J. Infrared Millimeter Waves* **2**, 373 (1981).
14. J.A. Davies, *Phys. Fluids B* **1**, 663 (1989).
15. A.T. Lin, and C.C. Lin, *Phys. Fluides B* **1**, 2286 (1989).
16. L.R. Barnett et al., *Phys. Rev. Lett.* **63**, 1062 (1989).
17. K.R. Chu et al., *Phys. Fluids B,* **3**, 2403 (1991)
18. K.R. Chu, and A.T. Lin, *IEEE Trans. Plasma Science* **16**, 90 (1988).
19. K.R. Chu et al., *Phys. Rev. Lett.* **74**, 1103 (1995).
20. Y.Y. Lau, K.R. Chu, and L.R. Barnett, *Int. J. Infrared and Millimeter Waves* **2**, 395 (1981).
21. P. Sprangle, and W.M. Manheimer, *Phys. Fluids* **18**, 224 (1975).
22. A.K. Ganguly, and S. Ahn, *Int. J. Electron.* **53**,641 (1982).
23. Fliflet, A. W., *Int. J. Electron.* **61**, 1049 (1986).
24. C.S. Kou et al., *IEEE Trans. Plasma Science* **20**, 155 (1992)
25. Ch Wang et al., *Rev. Sci. Instru.* **68**, 3031 (1997).
26. A.T. Lin et al., *Int. J. Electron.* **72**, 873 (1992).